Journal of Sound and Vibration (2000) **238**(2), 327–350
doi:10.1006/jsvi.2000.3207, available online at http://www.idealibrary.com on IDEAL®

MODEL REDUCTION AND FREQUENCY WINDOWING FOR ACOUSTIC FEM ANALYSIS

R. P. INGEL

Naval Research Laboratory, Code 6354, 4555 Overlook Avenue, SW Washington, DC 20375-5343, U.S.A.

C. T. DYKA

NAVSEA, Indian Head, 101 Strauss Avenue, Indian Head MD 20640-5053, U.S.A.

AND

L. D. FLIPPEN, JR.

Naval Research Laboratory, Code 6354, 4555 Overlook Avenue, SW Washington, DC 20375-5343, U.S.A.

(*Received* 30 *September* 1999, *and in final form* 21 *June* 2000)

Model degrees-of-freedom reduction and frequency windowing via interpolation are combined for application to acoustic finite element analysis problems. Projection operators are employed for the model reduction or condensation process. Interpolation is then introduced over a user defined frequency window, which can have real and imaginary boundaries and be quite large. Hermitian interpolation functions (which require derivative information) as well as standard Lagrangian functions, which can be linear, quadratic or cubic, have been used to construct the windows. For one-dimensional windows, the location of interior evaluation points can be varied to increase accuracy. Results are excellent for example problems, even for large d.o.f. reduction and large frequency windows containing numerous resonances (eigenvalues). The reduced models within the windows appear to indicate accurately the location of the resonances.

1. INTRODUCTION

The efficient and accurate solution of large degree-of-freedom (d.o.f.) problems remains difficult for linear, dynamic and steady state analyses. Many problems have become very large and complex to solve in an economic fashion, especially if, for example, a large number of frequency responses are required for a structural acoustic analysis. In addition, the problem of the interaction of scales, which can extend from the micro- to the macro-scale, has not been adequately addressed. This is especially true for an heterogeneous media such as composite materials and structures. For linear problems, the use of substructuring methods [1, 2] can be very effective. However, when applied to acoustic steady state analyses, substructuring methods introduce further approximations and still require the solution of the reduced problem at each desired frequency.

Flippen [3, 4] has developed a general-purpose, dynamic, condensation model reduction (CMR) theory which utilizes projection operators on governing differential equations. This approach allows general d.o.f. reduction in spatially discretized models of heterogeneous material and is not restricted to periodic media or other homogenization assumption. The

0022-460X/00/470327 + 24 $35.00/0

CMR method is applicable to general second order differential equations in time. This methodology [5] was implemented in a linear finite element environment and applied to dynamic analysis (time domain) of transient elasticity problems.

In reference [6], Flippen extended this condensation model reduction (CMR) theory to include frequency domain analysis. The use of projection operators on the governing differential equations allowed interpolation across selected frequency windows to be accomplished. Hermitian interpolation function [1], which required derivative information on the boundaries of the frequency window, were used. The CMR method was applied to structural acoustics analysis and was implemented into a one-dimensional (1D) finite-volume environment. The method was applied to a complex 1D composite structure and good results were obtained across wide-frequency windows for the reduced d.o.f. solutions as compared to the full d.o.f. solution. The eigenvalues of the reduced system were found to match quite well with those of the full system, even for significant d.o.f. reduction. In this particular article, a method was developed (though not implemented) to account for singularities caused by resonances using singularity decomposition techniques. In a recent effort, Flippen [7] has extended this work into a general model reduction theory, which unites and generalizes the reduced basis and frequency window class of methods as submethods.

In this present work, the CMR method has been extended to frequency windowing directly into a 2D and 3D finite element method (FEM) environment and applied to structural acoustics. The method is referred to as the frequency window reduction (FWR) method for d.o.f. reduction of spatially discrete time-transformed linear models. In this case frequency windows are chosen in which a discretized model can be reduced in its d.o.f. The method consists of discretizing a FEM model and selecting the "master" node point d.o.f.s, which are to be retained in the analysis. The contribution of the "slave" node points, which are to be condensed out, is reformulated and is used to generate an interpolation of the functional dependence of the "slave" response across a selected frequency window. A "reduced" system operator now may be constructed, which consists of the "master" d.o.f.s, and the influence of the interpolated "slave" response. The reduced system response can then be solved across a selected frequency interpolation window.

In addition to the Hermitian interpolation functions (two-point interpolation) of the "slave" response first employed with this method [6], standard Lagrangian interpolation functions (linear, quadratic and cubic not requiring derivative calculations) have been included [8]. These latter functions, which do not require derivative information at the evaluation points, are an important addition that are far simpler to implement, very efficient and provide function evaluation within the window of interest that can increase accuracy. Also, for the standard quadratic and cubic interpolation schemes, the location of the evaluation points that are within the interior of the frequency window can be varied for a 1D frequency window (a line in frequency space). This is an important capability that can substantially increase the accuracy within the selected regions and within the interpolation window. The use of evaluation points within the window was extended to include higher order Hermitian functions with one and two interior interpolation evaluation points for 1D windows. This led to a further improvement in accuracy.

Computational analyses were performed using a program developed in Fortran 90 which can read in and solve third party generated finite element models. Two-dimensional results from the FWR program are presented and show excellent results for the "reduced" system solutions as compared to the full d.o.f. solutions. Accurate results are obtained for large d.o.f. reduction and large-frequency windows, even while not explicitly accounting for the presence of numerous resonances (eigenvalues) within the window.

2. FWR FORMULATION FOR MECHANICAL SYSTEMS

For a discretized mechanical system, the governing equations of the equilibrium can be expressed in matrix form as

$$\mathbf{M}\frac{\partial^2 \mathbf{u}}{\partial t^2} + \mathbf{D}\frac{\partial \mathbf{u}}{\partial t} + \mathbf{K}\mathbf{u} = \mathbf{f}, \tag{1}$$

where **M**, **D** and **K** are the mass, damping and stiffness matrices, respectively, **u** are the system displacements and **f** are the system loads. Expressed in operator form equation (1) becomes

$$\mathbf{L}\mathbf{u} = \mathbf{f}, \tag{2}$$

in which the matrix of operator **L** is defined as

$$\mathbf{L} = \mathbf{M}\frac{\partial^2}{\partial t^2} + \mathbf{D}\frac{\partial}{\partial t} + \mathbf{K}. \tag{3}$$

The frequency domain is obtained from the exponential form of the Fourier transform, $F = e^{i\omega t}$, applied to equation (3), so that the operator **L** becomes

$$\hat{\mathbf{L}} \equiv -\omega^2\mathbf{M} + i\omega\mathbf{D} + \mathbf{K}. \tag{4}$$

The mechanical system operator $\hat{\mathbf{L}}$ is now a function of the continuous independent variable ω and equation (2) may then be explicitly rewritten as

$$\hat{\mathbf{L}}(\omega)\hat{\mathbf{u}}(\omega) = \hat{\mathbf{f}}(\omega). \tag{5}$$

The displacement and load terms in the above equation can be written in complex form as $\hat{\mathbf{u}} = |u|e^{i\omega t}$ and $\hat{\mathbf{f}} = |f|e^{i\omega t}$. Note that $i = \sqrt{-1}$.

Applying **P**, a permutation matrix operator [5], on the operator matrix $\hat{\mathbf{L}}$ in equation (4) as $\tilde{\mathbf{L}} = \mathbf{P}\mathbf{L}\mathbf{P}^{-1}$, such that $\hat{\mathbf{L}}$ can now be reordered and partitioned as

$$\tilde{\mathbf{L}} = \begin{pmatrix} \tilde{\mathbf{L}}_{11} & \tilde{\mathbf{L}}_{12} \\ \hat{\mathbf{L}}_{21} & \tilde{\mathbf{L}}_{22} \end{pmatrix}. \tag{6}$$

In this equation, the index "1" represents the "master" d.o.f. and the index "2" represents the "slave" d.o.f. The term "master" d.o.f. refers to the independent (retained) d.o.f.s of the reduced system in the FEM model. The master d.o.f.s are typically chosen as d.o.f.s, which have applied loads or constraints such as fixed boundary conditions in an FEM model. The term "slave" d.o.f. refers to the dependent d.o.f.s or those that are to be condensed or reduced out of the full FEM model. These are d.o.f.s which typically do not have applied loads or constraints. In general, the number of master d.o.f.s will be considerably less than the number of slave d.o.f.s. In addition, for the present work, it is assumed that any node which has an applied external loading or boundary condition is included in the list of master d.o.f.s.

The mechanical system operator, $\hat{\mathbf{L}}$ equation (4), may now be transformed using a *generalized* complex variable, $q = q_1 + iq_2$ by $q \equiv i\omega$, so that it becomes

$$\hat{\mathbf{L}}(q) = q^2\mathbf{M} + q\mathbf{D} + \mathbf{K}. \tag{7}$$

It is assumed that the matrices **M**, **D**, and **K** are *not* functions of the generalized variable q (or frequency ω). From this equation, the system operator $\tilde{\mathbf{L}}$ in the generalized complex variable is obtained from the partitioned operator matrix, equation (6), as

$$\tilde{\mathbf{L}} \equiv q^2 \begin{pmatrix} \tilde{\mathbf{M}}_{11} & \tilde{\mathbf{M}}_{12} \\ \tilde{\mathbf{M}}_{21} & \tilde{\mathbf{M}}_{22} \end{pmatrix} + q \begin{pmatrix} \tilde{\mathbf{D}}_{11} & \tilde{\mathbf{D}}_{12} \\ \tilde{\mathbf{D}}_{21} & \tilde{\mathbf{D}}_{22} \end{pmatrix} + \begin{pmatrix} \tilde{\mathbf{K}}_{11} & \tilde{\mathbf{K}}_{12} \\ \tilde{\mathbf{K}}_{21} & \tilde{\mathbf{K}}_{22} \end{pmatrix}. \tag{8}$$

Further applying the permutation matrix to the system stimuli, $\hat{f}$, according to

$$\mathbf{P} = \mathbf{P}^{-1} \begin{pmatrix} \mathbf{I} & 0 \\ \alpha & 0 \end{pmatrix} \mathbf{P}, \tag{9}$$

results in the system loads are being partitioned as

$$\tilde{\mathbf{f}} = \mathbf{P}\mathbf{f} = \begin{pmatrix} \tilde{\mathbf{f}}_m \\ \tilde{\mathbf{f}}_s \equiv \alpha \tilde{\mathbf{f}}_m \end{pmatrix}. \tag{10}$$

Here the subscripts "m" and "s" refer to the "master" and "slave" d.o.f.s respectively. The matrix α is defined such that $\tilde{\mathbf{f}}_s = \alpha \tilde{\mathbf{f}}_m$, and **I** is the identity matrix.

The α matrix, the "slave-master" response matrix, is an operator matrix, which is used to relate "slave" d.o.f. properties such as constraints, forces and applied loads to the master d.o.f.s. Usually slave d.o.f.s are chosen, which do *not* have constraints or loads. However, for very large complex FEM models, in order to reduce the total number of d.o.f.s, it may desirable to also condense out d.o.f.s which have constraints or applied loads. Hence, the α operator matrix can be used to interpolate from the "master" d.o.f.s for example an applied load or boundary condition to the "slave" d.o.f.s. In this present work it has been assumed that the α operator matrix is zero based on the choice of the "master" and "slave" d.o.f.s. However, the application of a non-zero α operator matrix as well as completely arbitrary constraint and loading conditions of the d.o.f.s will be the subject of future work.

3. DEGREE OF FREEDOM REDUCTION

The condensation model reduction (CMR) [3–6] theory has shown that the general d.o.f. reduction of an operator matrix may be obtained from the condensation equation

$$(\tilde{\mathbf{L}}_{22} - \alpha \tilde{\mathbf{L}}_{12})\beta = \alpha \tilde{\mathbf{L}}_{11} - \tilde{\mathbf{L}}_{21}, \tag{11}$$

where

$$\tilde{\mathbf{L}} = \begin{pmatrix} \tilde{\mathbf{L}}_{11} & \tilde{\mathbf{L}}_{12} \\ \tilde{\mathbf{L}}_{21} & \tilde{\mathbf{L}}_{22} \end{pmatrix}$$

is the reordered/partitioned operator matrix (6) and the α matrix, the "slave–master" response matrix, is defined. The goal is to solve for the β matrix in order to construct the reduced system operator. The complex β matrix in the generalized complex variable can be found directly as

$$\beta(q) = G^{-1}(q)H(q) \tag{12}$$

in which the G^{-1} matrix is the matrix inverse of

$$G(q) \equiv \tilde{\mathbf{L}}_{22}(q) - \alpha(q)\tilde{\mathbf{L}}_{12}(q) \tag{13a}$$

and the H matrix is

$$H(q) \equiv \alpha(q)\tilde{\mathbf{L}}_{11}(q) - \tilde{\mathbf{L}}_{21}(q). \tag{13b}$$

Having determined the form of β, the final "*reduced*" operator, $\bar{\mathbf{L}}_0$, may be also written explicitly as a function of the generalized variable as

$$\bar{\mathbf{L}}_0(q) = \tilde{\mathbf{L}}_{11}(q) + \tilde{\mathbf{L}}_{12}(q)\beta(q) \tag{14}$$

and hence the reduced system equation to be solved is

$$\bar{\mathbf{L}}_0(q)\mathbf{u}_m = \tilde{\mathbf{f}}_m, \tag{15}$$

where $\Pi\tilde{\mathbf{f}} = \tilde{\mathbf{f}}_m$ and $\Pi = (\mathbf{I}\ \mathbf{0})\mathbf{P}$. The column matrix (vector) $\mathbf{u}_m$ represents the "master" or independent d.o.f. system response. Finally, the "slave" response can be obtained directly from the "master" response by reconstruction via

$$u_s = \beta(q)u_m. \tag{16a}$$

Hence, the "total" reduced solution ("master" and reconstructed "slave" results) is then

$$\mathbf{u}_{Reduced} = \begin{pmatrix} \mathbf{u}_m \\ \mathbf{u}_s \end{pmatrix}. \tag{16b}$$

The goal in the general CMR method is to reduce the number of d.o.f., in order to allow efficient computational solutions to a problem, while maintaining good accuracy. The primary consideration is the accuracy of the reduced solution, as compared to the full system solution. Hence, there will be trade-offs among the degree of reduction, e.g., the number of d.o.f.s condensed out from the full system, the computational efficiency and the accuracy of the reduced solution.

In order to obtain the reduced system operator, equation (14), $\bar{\mathbf{L}}_0(q)$, it is necessary to determine $\beta(q)$ from equations (12) and (13), $G^{-1}(q)$ at *every* point, q (or frequency). This requires the $G^{-1}(q)$ matrix to be calculated at *every* solution point in order to determine $\beta(q)$. It is desired to minimize the work necessary in obtaining $G^{-1}(q)$ at every point q, since the inversion of $G(q)$ would involve inverting a "slave" d.o.f. by a "slave" d.o.f. sized matrix each point. So, rather than determine $G^{-1}(q)$ at *every* solution point, a method has been devised in order to obtain an interpolated $\hat{G}^{-1}(q)$, to be valid within a specified frequency "window". This may be expressed as

$$\beta(q) \cong \hat{G}^{-1}(q)\, H(q). \tag{17}$$

Two methods, Hermitian interpolation and Lagrangian shape function interpolation are employed to interpolate $\hat{G}^{-1}(q)$ at points within a window based on the assumption that $G^{-1}(q)$ is a relatively smooth varying function of q within the bounds of the defining window. This assumes that any eigenvalues, which are within the defining window, do not significantly affect the smooth interpolation of $G^{-1}(q)$. The interpolation method of $\hat{G}^{-1}(q)$ allows the formulation and calculation of the interpolation or "constructor" matrices prior

to any solution. These matrices are then valid for any point within the window. Hence, the main work involved in the matrix inversion and matrix interpolation calculations can be performed as pre-processing steps. This approach can significantly reduce the amount of computation required to generate the reduced system operator, $\bar{\mathbf{L}}_0$, and solve the reduced system equation, (15). The reduced computation required for the solution of equation (15) would allow more frequencies and loading conditions to be examined within an interpolation window at reduced computational costs.

4. INTERPOLATION METHODS FOR A FREQUENCY WINDOW

Hermitian [5] and standard Lagrangian [8] (linear, quadratic and cubic) interpolation methods have been implemented to interpolate $G^{-1}(q)$. It is assumed that $G^{-1}(q)$ is a relatively smooth varying function of q (or frequency) within the bounds of the window. Also it is assumed that within the window, the interpolation of $G^{-1}(q)$ is not affected by the presence of eigenvalues. Based upon our experience to date, this latter assumption is appropriate.

The Hermitian method for the interpolation of $\hat{G}^{-1}(q)$ requires the determination of $G(q)$ as defined by equation (13a), its inverse, $G^{-1}(q)$, and the derivatives of $G^{-1}(q)$ with respect to $\bar{q}_i$, at the points defining the interpolation window. The bi-cubic Hermitian interpolation of a rectangular 2D window as well as a generalized Hermitian interpolation of a 1D linear window (line) have been used to approximate $\hat{G}^{-1}(q)$ at any point q within a window defined by the interpolation points $\bar{q}_i$. Both of these methods have been implemented, however, only the 1D Hermitian interpolation method will be discussed here. The reader is referred to reference [9] for further details.

The generalized 1D Hermitian interpolation method may be used to approximate $\hat{G}^{-1}(q)$ at any point, q, as

$$\hat{G}^{-1}(q) = W_1(\bar{q}) + q\,W_2(\bar{q}) + q^2\,W_3(\bar{q}) + \cdots + q^{[(Order+1)N]-1}\,W_{(Order+1)N}(\bar{q}), \tag{18}$$

where $\bar{q}$ are the N number of interpolation points and the *Order* represents the number of derivatives of the function required for the interpolation. However, here, we shall restrict the analysis to first order Hermitian interpolation with up to 4 interpolation points. For a first order Hermitian interpolation, there will be $2N$, i.e., $(Order+1)N$, W_i "constructor" matrices needed for the approximation of $\hat{G}^{-1}(q)$ in equation (18). These matrices may be calculated as

$$\begin{pmatrix} W_1 \\ W_2 \\ \vdots \\ W_{2N} \end{pmatrix} = B^{-1}(\bar{q}) \circ \begin{pmatrix} G^{-1}(\bar{q}_1) \\ \dfrac{\partial G^{-1}(\bar{q}_1)}{\partial q} \\ G^{-1}(\bar{q}_2) \\ \dfrac{\partial G^{-1}(\bar{q}_2)}{\partial q} \\ \vdots \\ G^{-1}(\bar{q}_N) \\ \dfrac{\partial G^{-1}(\bar{q}_N)}{\partial q} \end{pmatrix}. \tag{19}$$

In the above equation, the derivatives as well as function evaluation at the boundaries of the frequency window and at any interior interpolation points are required. In reference [6], the following approximation for the first derivative of $G^{-1}(q)$ with respect to q was successfully introduced:

$$\frac{\partial[G^{-1}(q)]}{\partial q_j} \cong -G^{-1}(q)\frac{\partial G(q)}{\partial q_j}G^{-1}(q), \tag{20}$$

where $G^{-1}(q)$ is the matrix inverse of $G(q)$ as defined in equation (13a). The interpolation coefficient matrix $B(\bar{q}_j)$ is calculated from the matrix as

$$B(\bar{q}) = \begin{Bmatrix} \vartheta(\bar{q}_1) \\ \dfrac{\partial \vartheta(\bar{q}_1)}{\partial q} \\ \vartheta(\bar{q}_2) \\ \dfrac{\partial \vartheta(\bar{q}_2)}{\partial q} \\ \vdots \\ \vartheta(\bar{q}_N) \\ \dfrac{\partial \vartheta(\bar{q}_N)}{\partial q} \end{Bmatrix}, \tag{21}$$

defining $a \equiv (Order + 1)N - 1$ and the following coefficient vectors at each of the N interpolation points, $\bar{q}_i$:

$$\vartheta(\bar{q}_i) = (1, \bar{q}_i, \bar{q}_i^2, \bar{q}_i^3, \bar{q}_i^4, \ldots, \bar{q}_i^a), \quad \frac{\partial \vartheta(\bar{q}_i)}{\partial q_i} = (0, 1, 2\bar{q}_i, 3\bar{q}_i^2, 4\bar{q}_i^3, \ldots, a\bar{q}_i^{a-1}). \tag{22}$$

From equation (21) the inverse may be easily obtained and used to calculate the "constructor" matrices of equation (19). These matrices now may be used to calculate via equation (18), the interpolated $\hat{G}^{-1}(q)$ at any point within the window.

For the Lagrangian interpolation method, isoparametric 2D quadratic (or cubic) shape functions of a rectangular "element" can be used to interpolate any point within the element. A rectangular FEM element with 4 to 9 (or 16) nodes may be used to represent the frequency window to be interpolated. Also, isoparametric 1D shape functions of a linear "element" can be used to interpolate any point along a selected line. A 1D linear element with 2 to 4 nodes is used to represent a line either along or parallel to the "real" *or* the "imaginary" frequency axes. The value of $\hat{G}^{-1}(q)$ can then be interpolated by the shape functions evaluated at q from the 2D isoparametric co-ordinates (r, s) and the $G^{-1}(q)$ matrices previously calculated at each of the window interpolation points, $\bar{q}_i$, by

$$\hat{G}^{-1}(q) = \sum_{i=1}^{\#=4\text{ to }9,16} h_i(r, s)G_i^{-1}(\bar{q}) \tag{23}$$

or from the 1D isoparametric co-ordinate r and the $G^{-1}(\bar{q}_j)$ by

$$\hat{G}^{-1}(q) = \sum_{i=1}^{\#=2,3\text{ or }4} h_i(r)\, G_i^{-1}(\bar{q}). \tag{24}$$

As with the Hermitian interpolation, only 1D linear interpolations confined to the real frequency axes are presented (ω, the loading frequency is real, but the response of the system can be complex).

An additional capability included in both the standard Lagrangian and Hermitian interpolation functions was the ability to vary the position of the interior evaluation points within the frequency window for 1D interpolation only, in which case the window becomes a line. The ability to vary the position of the interior evaluation can further improve the accuracy by effectively producing a window within a window.

5. IMPLEMENTATION INTO A FEM ENVIRONMENT

As in our earlier work [5] on model reduction, the use of projection operators for model reduction coupled with a complex frequency windowing method required to build our own finite element program for frequency window reduction (FWR), to demonstrate the utility and accuracy of this new approach. FWR is written in portable Fortran 90 [10] to take the advantage of this rich programming environment, especially for matrix manipulations, dynamic memory allocation, new constructs such as name lists, and to help this work transition to a parallel environment in future.

Initially, the FEM models were generated by the FWR program. The ABAQUS FEM program [11] was then used to check the original FWR models and to develop further FEM models for use in the FWR method. The global mass and stiffness matrices for the models used in these examples were generated by ABAQUS and imported into the FWR programs. FWR requires the co-ordinates of the nodes; element types (for d.o.f. per node) and connectivity; either the global or local element stiffness, mass or damping matrices; and loading or constraint information. Then these matrices were reordered and partitioned according to the user-defined choices of "master"node points by the FWR program. This approach allows much more flexibility for the development of the FWR program, without the need for building a more general-purpose internal finite element capability directly into FWR.

Calculations were performed using both the Hermitian and Lagrangian interpolation methods in order to obtain a reduced solution via equations (15) and (16) for direct comparison to solutions of the full d.o.f. model, equation (5). The interpolation method for a 2D rectangular window [9] was performed on several examples. However, since the frequency sweep calculations were confined to the real frequency axis only, the 2D analyses gave identical results when compared to the appropriate 1D analyses. The 2D Hermitian interpolation method has two interpolation (inversion) points on the real axis, hence its results were the same as the 1D two point (2^{pt}) Hermitian interpolation method. Similarly, the 2D Lagrangian method, which has three interpolation points on the real frequency axis, was identical to the 1D three-point (3^{pt}) Lagrangian method.

In all the following examples, results are shown for the 1D line interpolation method confined to the real frequency axis. Also, the analyses for all examples were performed using the higher point interpolations, four-point (4^{pt}) Hermitian and four-point (4^{pt}) Lagrangian. These methods gave more accurate results for comparison to the full d.o.f. solutions.

Error analysis was performed utilizing the relative error of the infinity norms of the solution matrices. The relative error is defined as

$$\text{Relative Error} = \frac{\|(\mathbf{u}_{reduced} - \mathbf{u}_{full})\|_\infty}{\|\mathbf{u}_{full}\|_\infty}, \tag{25}$$

where $\mathbf{u}_{reduced}$ and $\mathbf{u}_{full}$ are the displacement magnitudes for the reduced and full d.o.f. problem, respectively, and represent the entire solution. The infinity norm of an $m \times n$ matrix, $\mathbf{A}$, is defined as $\|\mathbf{A}\|_\infty = \max_{1 \leqslant i \leqslant m} \sum_{j=1}^{n} |\mathbf{a}_{ij}|$. The relative error as defined above is a measure of the decimal digit precision of $\mathbf{u}_{reduced}$ as compared to $\mathbf{u}_{full}$. This relative error represents a stringent global error estimate.

The magnitude of the displacement for individual d.o.f.s as obtained from the full d.o.f. solution and as well as from the FWR interpolation reduced solutions were compared. Error analysis was performed on specific d.o.f.s to directly compare these solutions. The $\Delta\%$ or the percent error is defined as

$$\Delta\% = \left(\frac{|\mathbf{u}_{reduced} - \mathbf{u}_{full}|}{|\mathbf{u}_{full}|} \right)_{\text{d.o.f.}} 100, \tag{26}$$

where $\mathbf{u}_{reduced}$ and $\mathbf{u}_{full}$ here represent the magnitude of the displacement solution of a specific individual d.o.f. Also the averages of both the relative error and % error across the entire frequency window were done in order to summarize and compare specific results.

6. RESULTS

6.1. 2D THREE-LAYER LAMINATE

A 2D model of a three-layer laminate is presented as a first example. The laminate was comprised of layers of steel and polystyrene, as shown in Figure 1. The properties used in the model were 256·7 GPa as Young's modulus, 0·25 as Poisson's ratio, a density of 7900 kg/m^3 for the steel; and 9·387 GPa as Young's modulus, 0·25 as Poisson's ratio and a density of 1050 kg/m^3 for the polystyrene. The FEM model was formed from 88 ABAQUS 2D plain stress elements consisting of 115 node points representing 230 d.o.f.s (two-degrees-of-freedom per node point). Thirty-five "master" nodes with (2-d.o.f.) per node (70 d.o.f.s) were chosen and are shown in the figure as "•" symbols. These were selected as loaded and constrained node points and as material interfaces and material midpoints. This represents a 70% reduction in the d.o.f., i.e, 230-d.o.f.s for the full model to 70-d.o.f.s for the reduced problem.

Interpolation windows comparing the different interpolation methods for both full and partial frequency window sweeps are summarized in Table 1. Generally, from the table as

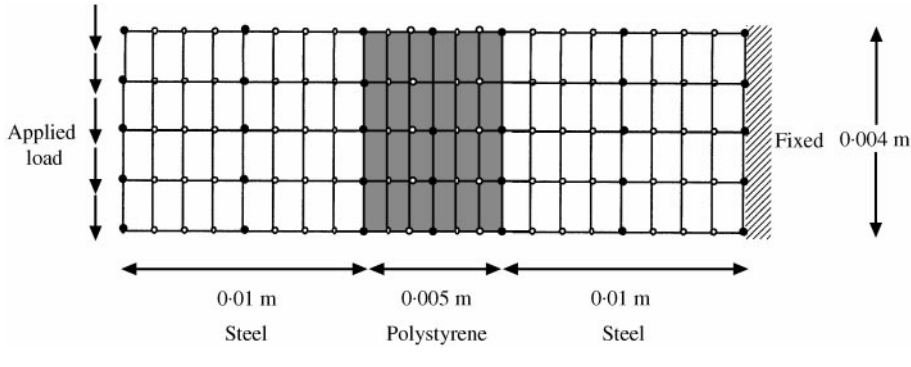

Figure 1. Three-layer steel-polystyrene laminate 2D model.

TABLE 1

Frequency interpolation window analysis for 2D laminate model

Frequency Range (kHz)	⟨Relative error⟩			⟨% error⟩ of d.o.f.			d.o.f.‡
	4^{pt} Lagrangian	4^{pt} Hermitian	2^{pt} Hermitian	4^{pt} Lagrangian	4^{pt} Hermitian	2^{pt} Hermitian	
0–10	$8{\cdot}9468 \times 10^{-2}$	$9{\cdot}9113 \times 10^{-6}$	$1{\cdot}4631 \times 10^{-1}$	13·1839	$1{\cdot}9479 \times 10^{-3}$	21·0456	$\|u\|_{1x}$
0–5	$1{\cdot}2757 \times 10^{-2}$	$5{\cdot}3985 \times 10^{-8}$	$2{\cdot}1946 \times 10^{-2}$	1·5983	$7{\cdot}5272 \times 10^{-6}$	3·2371	$\|u\|_{1x}$
				1·6126	$7{\cdot}3496 \times 10^{-6}$	3·5791	$\|u\|_{11x}$
0–5†	$5{\cdot}3469 \times 10^{-3}$	$2{\cdot}6331 \times 10^{-7}$	$6{\cdot}6452 \times 10^{-2}$	$5{\cdot}3999 \times 10^{-1}$	$2{\cdot}6190 \times 10^{-6}$	6·8923	$\|u\|_{1x}$
				$5{\cdot}4079 \times 10^{-1}$	$2{\cdot}6076 \times 10^{-6}$	6·9612	$\|u\|_{11x}$
0–3	$3{\cdot}5339 \times 10^{-3}$	$1{\cdot}9719 \times 10^{-9}$	$5{\cdot}0678 \times 10^{-3}$	$3{\cdot}8868 \times 10^{-1}$	$2{\cdot}0958 \times 10^{-7}$	1·0189	$\|u\|_{1x}$
				$4{\cdot}1186 \times 10^{-1}$	$2{\cdot}2025 \times 10^{-7}$	1·2206	$\|u\|_{11x}$
0–3†	$4{\cdot}2943 \times 10^{-4}$	$1{\cdot}7130 \times 10^{-10}$	$6{\cdot}0678 \times 10^{-3}$	$4{\cdot}5839 \times 10^{-2}$	$1{\cdot}9610 \times 10^{-8}$	$6{\cdot}4892 \times 10^{-1}$	$\|u\|_{1x}$
				$4{\cdot}6741 \times 10^{-2}$	$2{\cdot}0058 \times 10^{-8}$	$6{\cdot}6201 \times 10^{-1}$	$\|u\|_{11x}$

† Prtial frequency sweeps 1·5–2·5 kHz within the frequency interpolation window at a step size of 5 Hz.
‡ $|u|_{1x}$ is a "master" d.o.f. solution and $|u|_{11x}$ is a reconstructed "slave" d.o.f. solution via equation (16).

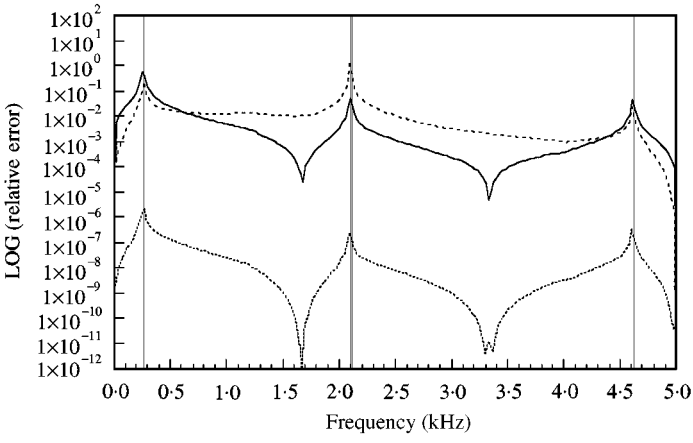

Figure 2. Relative error comparing the 4[pt] Lagrangian interpolation (——), the 4[pt] Hermitian interpolation (- - - -), and the 2[pt] Hermitian interpolation (– – – –) methods for the window range 0–5 kHz and a step size of 25 Hz.

expected, a decrease in the interpolation window size increases the accuracy of the reduced system response, i.e. a smaller error as compared to the full d.o.f. solution. This arises from the increased accuracy of the interpolation function and the ability to use smaller-frequency step sizes across the window. It can also be seen that the 4[pt] Lagrangian, because of the interior point information, is more accurate that the 2[pt] Hermitian, even though the Hermitian has derivative information at the interpolation (end) points. Clearly, the 4[pt] Hermitian, with both interior point and derivative information, has the lowest associated error.

For the frequency window range 0–5 kHz, a full frequency sweep was examined with step size of 25 Hz. The relative error plotted in Figure 2 for this interpolation window compares the Lagrangian and Hermitian interpolation functions over the entire interpolated window. It should be noted that at the end points and the two interior points (approximately 1·667 and 3·333 kHz) the error is very small. This is because these are points at which the inverse, $G^{-1}(q)$, is obtained directly, hence the solution is nearly exact. From this figure, the 4[pt] Lagrangian can be seen to have approximately the same error as the 2[pt] Hermitian, even though derivative information is contained in the Hermitian interpolation. However, it is obvious that the 4[pt] Hermitian has a significantly lower relative error, as well as capturing more accurately the eigenvalues or resonances of the system. The gray vertical lines in the figure represent the calculated constrained eigenvalues of the full d.o.f. model (see Table 2). It can be shown that the eigenvalues of the reduced d.o.f. model are nearly the same as those of the full d.o.f. model, although not identical.

The % error of the resultant displacement magnitude for the "master" d.o.f. 1_x is shown in Figure 3. This figure shows the overall accuracy as well as the errors associated near the resonances of the system. The 4[pt] Lagrangian and the 2[pt] Hermitian interpolation functions show errors of approximately 1%, as compared to the full d.o.f. solution. However, the 4[pt] Hermitian method has an extremely small error (1×10^{-5}) over the entire frequency range at a 70% d.o.f. reduction. The comparison of the 4[pt] Lagrangian and the 4[pt] Hermitian interpolation to the full d.o.f. solution for the displacement magnitude for the "master" d.o.f. 1_x is shown in Figure 4. Both interpolation methods produce the excellent agreement, as compared to the full d.o.f. response.

The results from the 4[pt] Hermitian interpolation method are indistinguishable from those for the full d.o.f. response. The % error as well as the actual magnitude of the "reconstructed" response for the "slave" d.o.f. 15_x, as expected, are identical to that for

TABLE 2

Calculated eigenvalues for the full d.o.f. model

Unconstrained eigenvalues (Hz)	Constrained eigenvalues (Hz)
0·0114380	265·1966
0·0135609	2091·7864
0·0179301	2109·2300
1113·0007	4607·8162
3056·8175	11665·5341
3493·2803	15225·6105
11826·8041	16479·0445

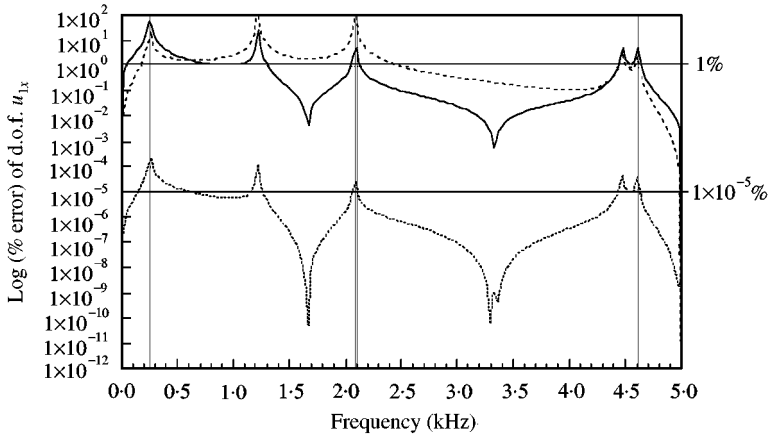

Figure 3. % error for the "master" d.o.f. 1_x comparing the 4[pt] Lagrangian interpolation (——), the 4[pt] Hermitian interpolation (- - - -), and the 2[pt] Hermitian interpolation (– – – –) methods for the window range 0–5 kHz and a step size of 25 Hz.

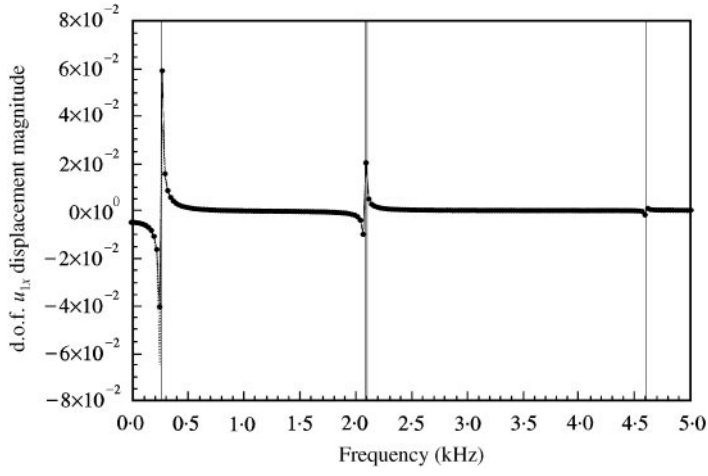

Figure 4. The "master" d.o.f. 1_x displacement magnitude comparing the $|u|_{1x}$ response for the full d.o.f. solution (——) and the reduced d.o.f. solutions: (- - - -), $|u|_{1x}$ response for the 4[pt] Lagrangian interpolation method; (●) response for the 4[pt] Hermitian interpolation method.

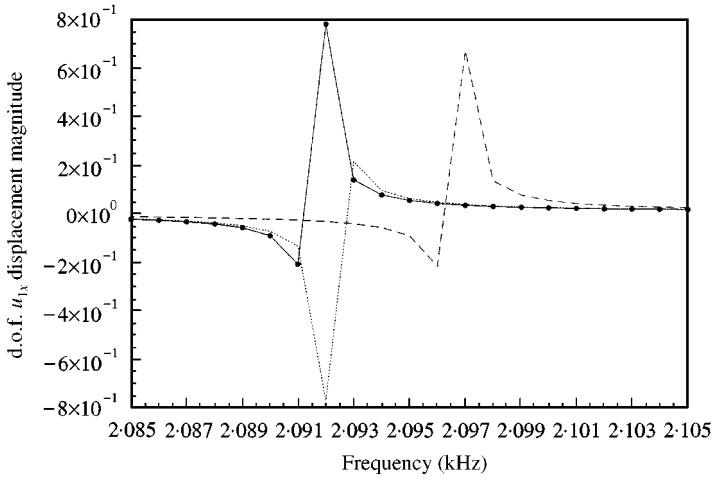

Figure 5. Partial frequency sweep for the "master" d.o.f. 1_x comparing interpolation functions at a full d.o.f. system resonance: $|u|_{1x}$ response for the full d.o.f. solution; (----), $|u|_{1x}$ response for the 4[pt] Lagrangian interpolation method; (– – – –) , response for the 2[pt] Hermitian interpolation method. Note: the response for the 4[pt] Hermitian interpolation method (●) is identical to that of the full d.o.f. response.

TABLE 3

Variable interior interpolation point for frequency range 0–10 *kHz*

⟨Relative error⟩		⟨% error⟩ of "master" d.o.f. $\|u\|_{1x}$		Interpolation point location (kHz)
4[pt] Lagrangian	4[pt] Hermitian	4[pt] Lagrangian	4[pt] Hermitian	
$8{\cdot}9468 \times 10^{-2}$	$9{\cdot}9113 \times 10^{-6}$	13·1839	$1{\cdot}9479 \times 10^{-3}$	3·333 and 6·667
$1{\cdot}1701 \times 10^{-1}$	$1{\cdot}1713 \times 10^{-5}$	14·0507	$2{\cdot}0283 \times 10^{-3}$	1·500 and 7·500
$6{\cdot}9364 \times 10^{-2}$	$2{\cdot}3604 \times 10^{-6}$	8·4686	$1{\cdot}0666 \times 10^{-3}$	1·500 and 4·000

"master" d.o.f.s, since the "slave" d.o.f. response is reconstructed directly from the "master" d.o.f. solution according to equation (16). Further reduction of the frequency window range, 0–3 kHz, was examined for a frequency sweep step size of 10 Hz. This smaller window improves both the overall accuracy by an order of magnitude and as well reduces the interpolation error associated with the resonances.

Using a frequency window range for the interpolation functions and only performing a partial sweep *within* the frequency window, it is possible to see more clearly the effects the different interpolation functions have near a resonance. For an interpolation window of 0–5 kHz but for a frequency sweep of 2·0–2·2 kHz with a step size of 1 Hz, the displacement magnitude for the "master" d.o.f. 1_x is shown in Figure 5. It is easily seen that the 4[pt] Lagrangian interpolation and the the 2[pt] Hermitian overshoot the eigenvalue. However, the 4[pt] Hermitian exactly matches the eigenvalue response based on the full d.o.f. solution.

It is possible within the FWR method to vary the placement of the interior interpolation (inversion) points for both the Lagrangian and Hermitian interpolation methods. In order to demonstrate this, a frequency window of 0–10 kHz with a step size of 50 Hz was examined by placing the interior points at different interior locations as summarized in Table 3. From this table, the error remains essentially the same for the variable

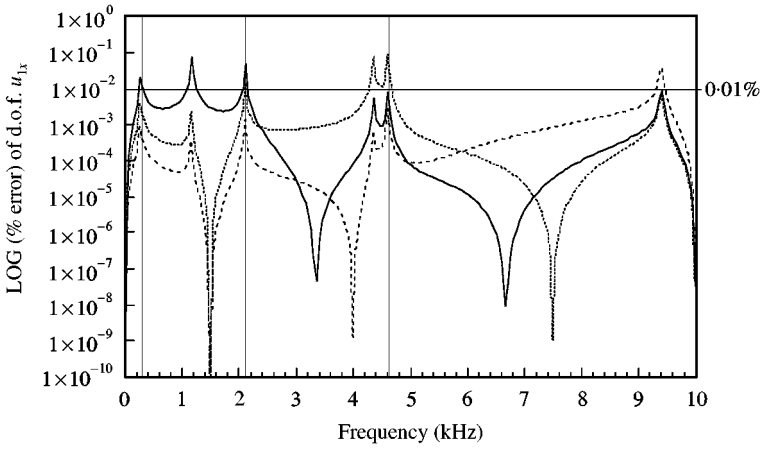

Figure 6. % error for the "master" d.o.f. 1_x comparing the 4[pt] Hermitian interpolation function for the range of 0–10 kHz and a step size of 50 Hz with variable interior point locations: (——), interior point locations (3·333 and 6·667 kHz); (- - - -), interior point locations (1·500 and 7·500 kHz); (– – – –), interior point locations (1·500 and 4·000 kHz).

placement of the interior interpolation points. The placement of the interior points does not generally reduce the *overall* error but reduces the error within the selected regions within a window. The variable placement does however tend to soften the error more uniformly across the entire window. This can most readily be seen in the % error of the displacement magnitude for the "master" d.o.f. 1_x for the Hermitian interpolation function in Figure 6. It is clear that the variable placement of the interior point does affect the error in smaller local frequency regions within the window. The selection of an interior point near eigenvalues tends to reduce the error associated with the resonance. There was no significant effect on the actual response and its accuracy, i.e., displacement magnitude for a particular d.o.f.

6.2. SPHERICAL HALF SHELL

The second example presented is a simple spherical shell as shown in Figure 7. The properties of the steel spherical shell were 180·0 GPa as Young's modulus, 0·333 as Poisson's ratio and a density of 7670 kg/m^3. A similar problem is discussed in the ABAQUS User's Manual [11]. The model is constructed using 50 quadratic axisymmetric SAX2 isoparametric shell elements for the undamped, free vibration problem. The total number of node points is 101, with 3 d.o.f.s per node point; hence, the total d.o.f.s for this model is 303. The number of "master" node points was chosen as 29, so the degree of reduction of the model is 71% (303–87-d.o.f.s). The selected "master" node points are shown in Figure 7 as "•" symbols (node nos. 1, 51 and 101) which represent the loaded and constrained nodes. The remaining "master" nodes were arbitrarily chosen from the model (node nos. 5, 9, 13, 17, 21, 25, 27, 29, 33 and 37).

A number of frequency interpolation windows were examined for this model, and the results are summarized in Table 4. For these analyses, only the 4[pt] Lagrangian and the 4[pt] Hermitian interpolation methods were used. Initially, large-frequency interpolation windows were examined with fairly coarse frequency sweep step sizes. As can be seen from the table, even for a very large window, 0–500 Hz, the Hermitian interpolation has a very

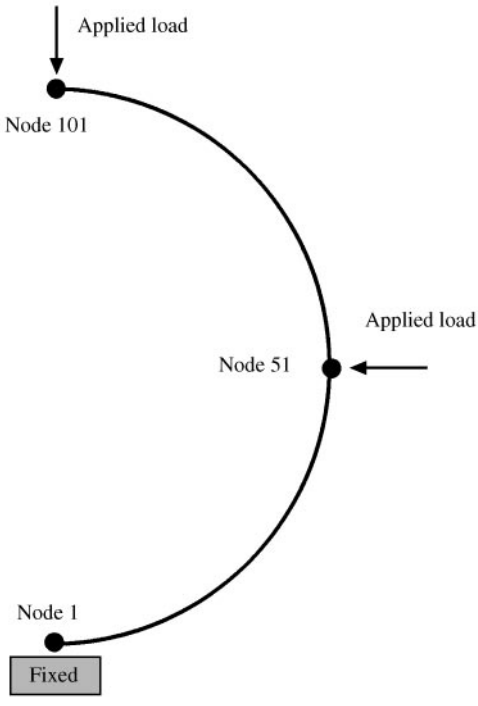

Figure 7. Spherical shell model.

low error, on the order of 0·01%. The relative error for an interpolation window of 0–300 Hz and frequency sweep step size of 1 Hz plotted in Figure 8. As can be seen in the figure, there are a very large number of eigenvalues within this window. Both interpolation functions capture the functional behavior at *all* of the eigenvalues, despite the large window and coarse step size. From Figure 9, the Lagrangian interpolation function shows a larger % error for the "master d.o.f. 51_x of approximately 1%, whereas the Hermitian shown an approximate error of only 0·001%. From this figure and the actual displacement magnitude the "master" d.o.f. 51_x, it can be seen that the functional behavior at every eigenvalue is represented. The response for other "master" and "slave" d.o.f.s showed identical behavior.

The frequency window size was now further reduced to 0–200 Hz with the sweep step size to 1 Hz. Within this particular window now only two eigenvalues are present near the end points of the window. A plot of the % error of "master" d.o.f. 51_x (Figure 10) shows a further decrease in the error from the previous window. The 4^{pt} Hermitian has an extreme accuracy in this frequency range, with a % error of less than 1×10^{-4}% at 71% d.o.f. reduction (Figure 10(a)). At these levels of accuracy, there is no discernable difference between the reduced interpolated solutions and the full d.o.f. solution. This same window range was then examined with a higher level of d.o.f. reduction of 303–29 d.o.f.s, or an 87% d.o.f. reduction. The relative error and the % error, shown in Figure 10(b), changed little, increasing by approximately one order of magnitude. Only a careful examination of the figure shows that the 4^{pt} Lagrangian does not exactly match the eigenvalue behavior at the low range of the frequency window. However, the error even for this significant reduction is surprisingly small, at 1% for the Lagrangian and 0·001% for the Hermitian methods.

As is seen in Figures 8 and 9 and from Table 5, there are large number of eigenvalues within the frequency range of 200–300 Hz. The frequency window range of 200–300 Hz was

TABLE 4

Frequency interpolation window analysis for spherical shell model

Frequency range (Hz) (d.o.f. % reduction)	⟨Relative error⟩		⟨% error⟩ of d.o.f.		d.o.f.†
	4^{pt} Lagrangian	4^{pt} Hermitian	4^{pt} Lagrangian	4^{pt} Hermitian	
0–500 (71%)	$3{\cdot}82455 \times 10^{-1}$	$1{\cdot}88293 \times 10^{-4}$	43·88975	$2{\cdot}45161 \times 10^{-2}$	$\|u\|_{51x}$
			84·89385	$4{\cdot}53325 \times 10^{-2}$	$\|u\|_{101y}$
			39·31291	$2{\cdot}13927 \times 10^{-2}$	$\|u\|_{75x}$
			48·19275	$2{\cdot}22450 \times 10^{-2}$	$\|u\|_{75y}$
			62·98936	$4{\cdot}18929 \times 10^{-2}$	$\|u\|_{75r}$
0–300 (71%)	$3{\cdot}85561 \times 10^{-2}$	$2{\cdot}70192 \times 10^{-6}$	4·47868	$3{\cdot}08129 \times 10^{-4}$	$\|u\|_{51x}$
0–200 (71%)	$8{\cdot}17052 \times 10^{-3}$	$6{\cdot}78324 \times 10^{-8}$	$9{\cdot}32031 \times 10^{-1}$	$8{\cdot}41653 \times 10^{-6}$	$\|u\|_{51x}$
			$7{\cdot}80872 \times 10^{-1}$	$7{\cdot}15517 \times 10^{-6}$	$\|u\|_{75x}$
100–200 (71%)	$9{\cdot}24500 \times 10^{-5}$	$5{\cdot}30811 \times 10^{-7}$	$1{\cdot}61164 \times 10^{-2}$	$1{\cdot}40703 \times 10^{-4}$	$\|u\|_{51x}$
200–300 (71%)	$1{\cdot}04594 \times 10^{-3}$	$4{\cdot}09726 \times 10^{-5}$	$1{\cdot}17638 \times 10^{-1}$	$5{\cdot}65539 \times 10^{-3}$	$\|u\|_{51x}$
0–200 and 200–300 (71%)‡	$4{\cdot}60823 \times 10^{-3}$	$2{\cdot}05202 \times 10^{-5}$	$5{\cdot}24834 \times 10^{-1}$	$2{\cdot}83190 \times 10^{-3}$	$\|u\|_{51x}$
100–200 and 200–300 (71%)§	$5{\cdot}69196 \times 10^{-4}$	$2{\cdot}07517 \times 10^{-5}$	$6{\cdot}68771 \times 10^{-2}$	$2{\cdot}89805 \times 10^{-3}$	$\|u\|_{51x}$
0–200 (71%)	$8{\cdot}17052 \times 10^{-3}$	$6{\cdot}78324 \times 10^{-8}$	$9{\cdot}32031 \times 10^{-1}$	$8{\cdot}41653 \times 10^{-6}$	$\|u\|_{51x}$
0–200 (87%)	$1{\cdot}05201 \times 10^{-1}$	$4{\cdot}15087 \times 10^{-5}$	11·94890	$5{\cdot}36735 \times 10^{-3}$	$\|u\|_{51x}$
200–300 (71%)	$1{\cdot}04594 \times 10^{-3}$	$4{\cdot}09726 \times 10^{-5}$	$1{\cdot}17638 \times 10^{-1}$	$5{\cdot}65539 \times 10^{-3}$	$\|u\|_{51x}$
200–300 (87%)	$7{\cdot}59079 \times 10^{-2}$	$1{\cdot}40523 \times 10^{-4}$	9·08258	$1{\cdot}45554 \times 10^{-2}$	$\|u\|_{51x}$

†$|u|_{51x}$ is a "master" d.o.f. solution and $|u|_{75x}$ is a reconstructed "slave" d.o.f. solution.
‡Results for frequency windows 0–200 Hz are combined with the results for 200–300 Hz
§Results for frequency windows 100–200 Hz are combined with the results for 200–300 Hz.

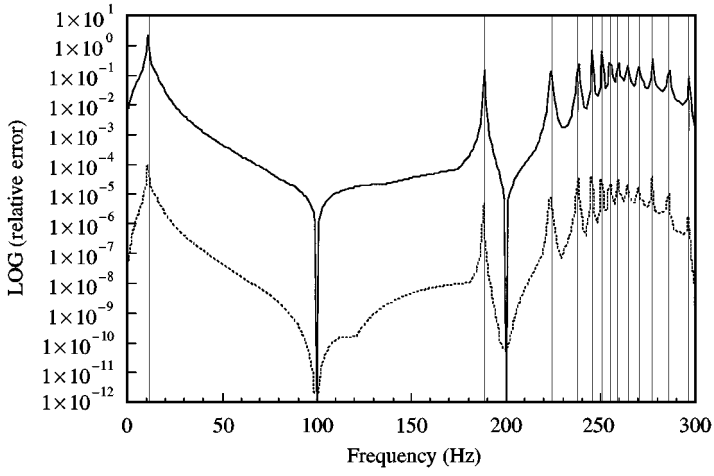

Figure 8. Relative error comparing the 4pt Lagrangian interpolation method (——) and the 4pt Hermitian interpolation method (- - - -) for the window range 0–300 Hz and a step size of 1 Hz.

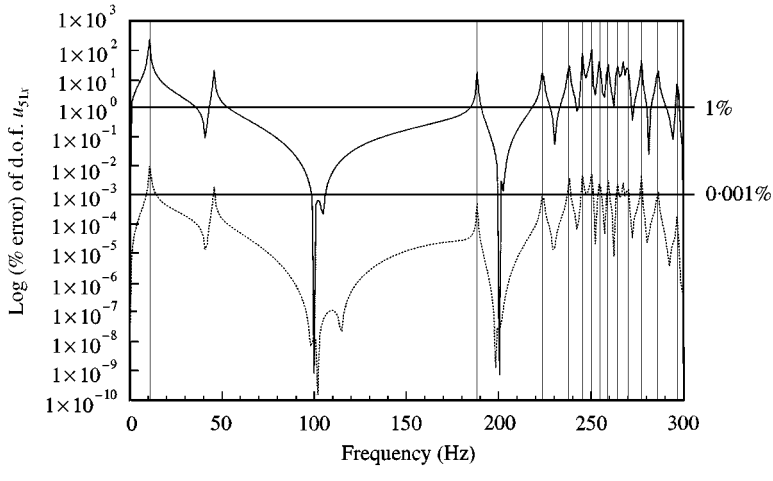

Figure 9. % error for the "master" d.o.f. 51_x comparing the 4pt Lagrangian interpolation method (——) and the 4pt Hermitian interpolation method (– – – –) for the window range 0–300 Hz and a step size of 1 Hz.

examined at both the 71% d.o.f. reduction and the 87% d.o.f. reduction level. This window range was chosen in order to characterize the behavior and accuracy of the FWR method with a large number of eigenvalues within a small interpolation window. Figure 11 shows the relative error at 71% reduction for the window range and the sweep step size of 0·5 Hz. Both interpolation methods result in a very low error of less than 1% over the entire window with highly accurate responses, as compared to the full d.o.f. solution. The characterization at 87% d.o.f. reduction showed identical trends as described above, with the error increasing by one order of magnitude. However, the Hermitian interpolation method still showed only an approximate error of 0·01% at 87% d.o.f. reduction. It should be noted that, as in the cases discussed above, *all* eigenvalue responses are clearly captured at both d.o.f. reduction levels.

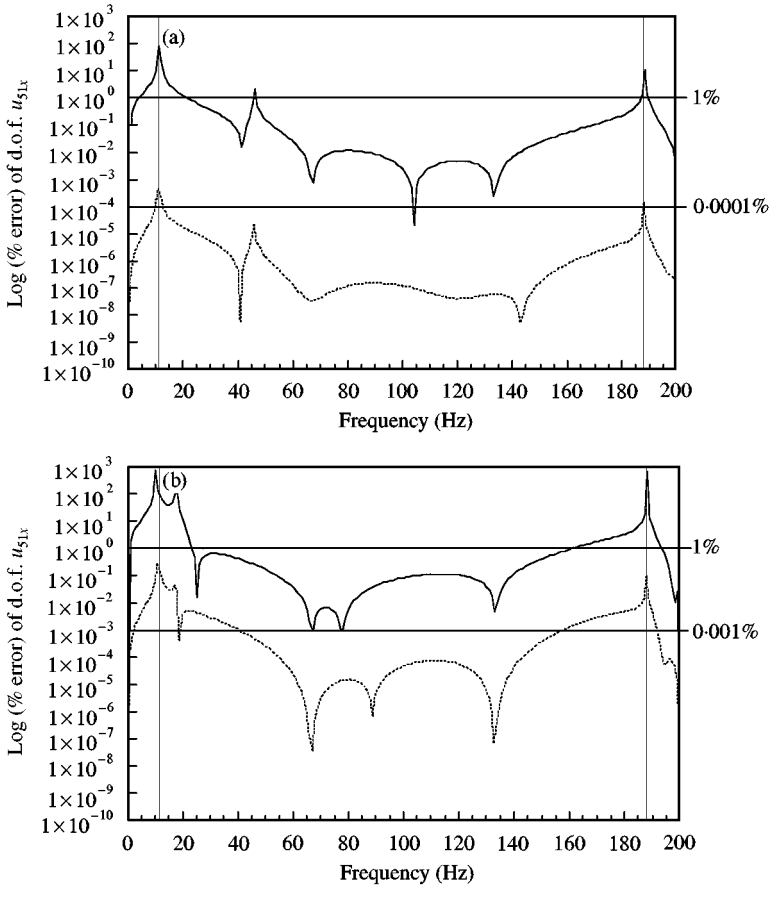

Figure 10. % error for the "master" d.o.f. 51_x at (a) 71% and (b) 87% d.o.f. reduction: (——), 4[pt] Lagrangian interpolation method; (– – – –), 4[pt] Hermitian interpolation method.

An important fact that can be observed with respect to the 4[pt] Hermitian interpolation curves in the above figure as is that the end interpolation (inversion) points of the frequency window does not approach a nearly zero value, as does the Lagrangian interpolation. It is important to note that the Hermitian interpolation method includes derivative information at all the interpolation points. As a result, if an eigenvalue is near an interpolation point particularly at the frequency window end points, the function and its derivative are rapidly varying near the point in the region of validity for the interpolation function. For this window range of 200–300 Hz, it can be seen from Table 5 or Figures 8 and 9, that there are eigenvalues lying just outside the interpolation window range (188·14 and 308·71 Hz). Hence, the influence from these eigenvalues, even though outside the interpolation region, does in fact contribute to the smoothness of the interpolation function and also to the accuracy of the response. The Lagrangian value should always be nearly zero at an interpolation (inversion) point.

Another very important point which applies to *all* the examples is that the eigenvalues of the system were *NOT* known beforehand. The constrained eigenvalues of the full d.o.f. models were calculated by standard routines [12] for comparison. Having shown how accurately the response of the reduced d.o.f. problem can be obtained, it is clear that the

TABLE 5

Calculated eigenvalues for the full d.o.f. model

Unconstrained eigenvalues (Hz)	Constrained eigenvalues (Hz)
11·258	9·805
187·36	188·14
222·69	223·48
236·95	237·73
244·41†	245·23
249·30	250·23
253·30†	254·44
257·26	258·75
267·02	263·68
273·53	269·63
281·49	276·87
291·12	285·68
302·59	296·24
316·06	308·71

† Used for Rayleigh damping calculation.

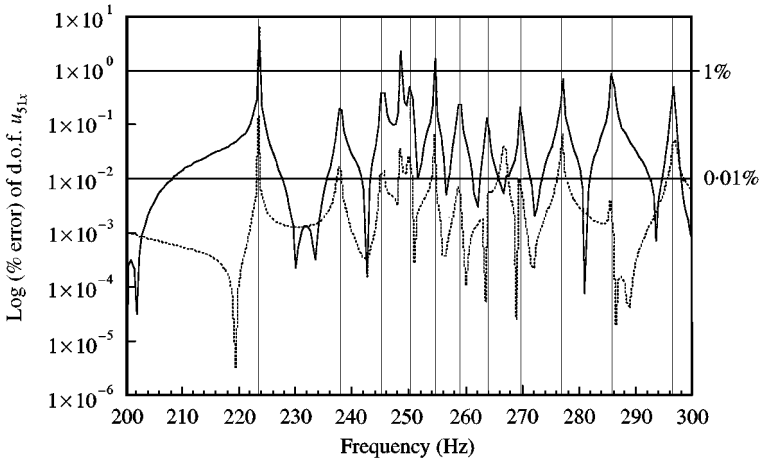

Figure 11. % error for the "master" d.o.f. 1_x comparing interpolation functions at 71% d.o.f. Reduction: (——), 4pt Lagrangian interpolation method; (- - - -), the 4pt Hermitian interpolation method.

eigenvalues of the full d.o.f. system may be closely approximated from the reduced d.o.f. model analysis. It is important to note that these eigenvalues represent the resonances of the "reduced" d.o.f. system, which generally are not significantly different from those of the full d.o.f. system.

One additional aspect of FWR method is that the multiple frequency windows may be analyzed independently and these solutions can then be combined to construct a large frequency response window. From the above analyses of the frequency windows of 0–200 Hz and 200–300 Hz can be combined and compared to the full analysis for the window range of 0–300 Hz. It is difficult to compare the overall accuracy (error) of the

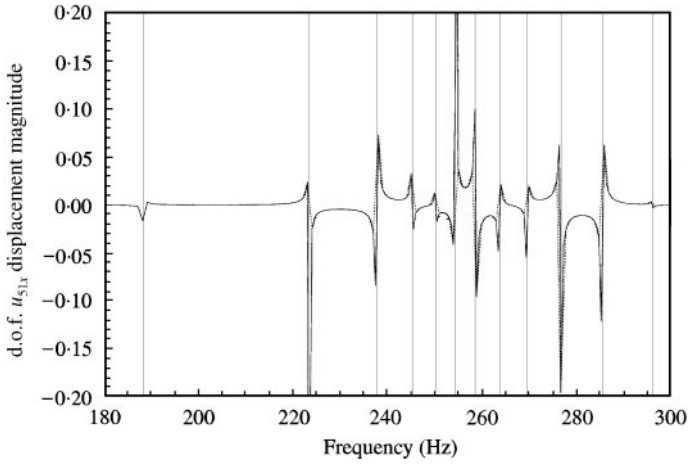

Figure 12. Displacement magnitude of the "master" d.o.f. 51_x for the range 0–300 Hz: (——) full d.o.f. response; (- - - -), 4^{pt} Hermitian response for the whole 0–300 Hz range; (– – – –), combined response for 0–200 Hz and 200–300 Hz ranges. Note expanded plot scale.

combined data as compared to the full frequency range because of the analyses, which are combined, have different parameters (window and step size). The accuracy of combined interpolation windows will strongly depend on the choice of parameters such as the window location, size and sweep step size. Also, as noted above, the presence of an eigenvalue near the interpolation window end points will affect the overall smoothness of the interpolated function. However, it is clear from Figure 12 that the responses of the displacement magnitude are nearly identical. Finally, this comparison of the combined responses of the window analysis, demonstrates again the consistency of the FWR method.

Rayleigh damping was then introduced into the spherical shell model. The mass and stiffness matrices were obtained from an ABAQUS model and reordered according to the selection of the "master" nodes. These matrices were then used to calculate the Rayleigh damping defined as

$$\mathbf{D} \equiv \bar{\alpha}\mathbf{M} + \bar{\beta}\mathbf{S}, \tag{27}$$

where the terms α and β are

$$\bar{\beta} = \frac{2(\omega_2\xi_2 - \omega_1\xi_1)}{\omega_2^2 - \omega_1^2}, \quad \bar{\alpha} = 2\omega_1\xi_1 - \bar{\beta}\omega_1^2 = \omega_1(2\xi_1 - \bar{\beta}\omega_1). \tag{28, 29}$$

Here, the terms ξ_1 and ξ_2 are the weightings or percentages of critical damping of the select frequency modes, ω_1 and ω_2. From the calculated eigenvalues of this model listed in Table 7, the frequency modes of $\omega_1 = 244{\cdot}41$ Hz and $\omega_2 = 253{\cdot}30$ Hz were chosen as being approximately in the middle of the interpolated frequency window range of 200–300 Hz. The calculated values for $\bar{\alpha}$ and $\bar{\beta}$ according to equations (28) and (29), at these selected eigenvalues, are summarized in Table 6 for different levels of critical damping (0·5, 1 and 5%).

Three different levels of Rayleigh damping were examined for the frequency window range of 200–300 Hz and are summarized in Table 7. Both real and imaginary solution

TABLE 6

Calculated values for $\bar{\alpha}$ and $\bar{\beta}$ at selected eigenvalues $\omega_1 = 244{\cdot}41\ Hz$ and $\omega_2 = 253{\cdot}30\ Hz$

ξ_1	ξ_2	$\bar{\alpha}$	$\bar{\beta}$
0·05	0·05	78·1552	$3{\cdot}1977 \times 10^{-5}$
0·01	0·01	15·6310	$6{\cdot}3955 \times 10^{-6}$
0·005	0·005	7·81552	$3{\cdot}1977 \times 10^{-6}$

TABLE 7

Frequency interpolation window analysis for spherical shell model with damping

Frequency range 200–300 Hz 71% d.o.f. reduction	⟨Relative error⟩		⟨% error⟩ of "master" d.o.f.$\lvert u\rvert_{51x}$	
	4^{pt} Lagrangian	4^{pt} Hermitian	4^{pt} Lagrangian	4^{pt} Hermitian
	Real		Real	
No damping	$1{\cdot}04594 \times 10^{-3}$	$4{\cdot}09726 \times 10^{-5}$	$1{\cdot}17638 \times 10^{-1}$	$5{\cdot}65539 \times 10^{-3}$
5% damping†	$1{\cdot}20912 \times 10^{-5}$	$2{\cdot}73770 \times 10^{-6}$	$4{\cdot}77508 \times 10^{-2}$	$2{\cdot}04404 \times 10^{-3}$
1% damping	$9{\cdot}17150 \times 10^{-5}$	$1{\cdot}31038 \times 10^{-5}$	$8{\cdot}71775 \times 10^{-2}$	$7{\cdot}72954 \times 10^{-3}$
0·5% damping	$2{\cdot}04280 \times 10^{-4}$	$1{\cdot}39016 \times 10^{-5}$	$5{\cdot}21610 \times 10^{-2}$	$3{\cdot}52020 \times 10^{-3}$
	Imaginary		Imaginary	
No damping	NA	NA	NA	NA
5% damping†	$3{\cdot}06675 \times 10^{-5}$	$3{\cdot}87553 \times 10^{-6}$	$3{\cdot}82516 \times 10^{-2}$	$2{\cdot}78551 \times 10^{-3}$
1% damping	$1{\cdot}80707 \times 10^{-4}$	$2{\cdot}34695 \times 10^{-5}$	$8{\cdot}15489 \times 10^{-2}$	$1{\cdot}20185 \times 10^{-2}$
0·5% damping	$3{\cdot}52384 \times 10^{-4}$	$2{\cdot}29230 \times 10^{-5}$	$1{\cdot}09397 \times 10^{-1}$	$9{\cdot}02209 \times 10^{-3}$

† Frequency step size 0·25 Hz. All other frequency step sizes were 0·5 Hz.

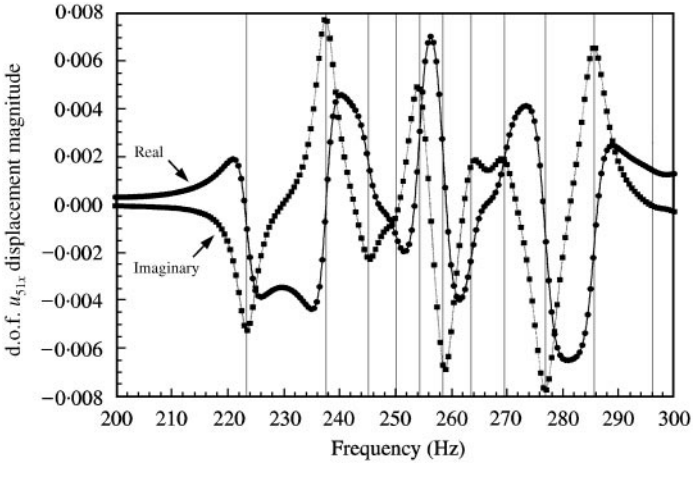

Figure 13. Real and imaginary displacement magnitudes for the "master" d.o.f. 51_x comparing the full d.o.f. solution response (——) to the 4^{pt} Hermitian interpolation method (●, ■) at 1% of critical Rayleigh damping.

responses are obtained. The error for both the real and imaginary solutions as compared to the full solution were small and the % error for the displacement magnitude of d.o.f. 51_x showed an error of less than 0·01%. Comparison of the error of the case in which damping *is* present to the case of *no* damping showed nearly the same % error. A comparison of the

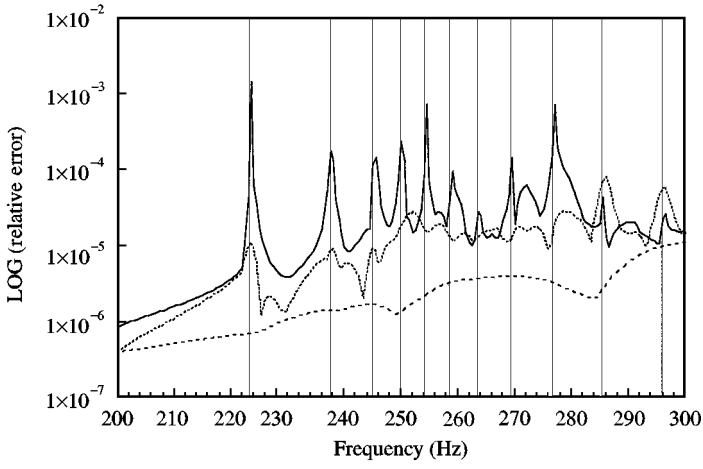

Figure 14. Real component of the relative error for the 4[pt] Hermitian interpolation method comparing no damping (——) to 1% damping (- - - -) and 5% damping (– – – –).

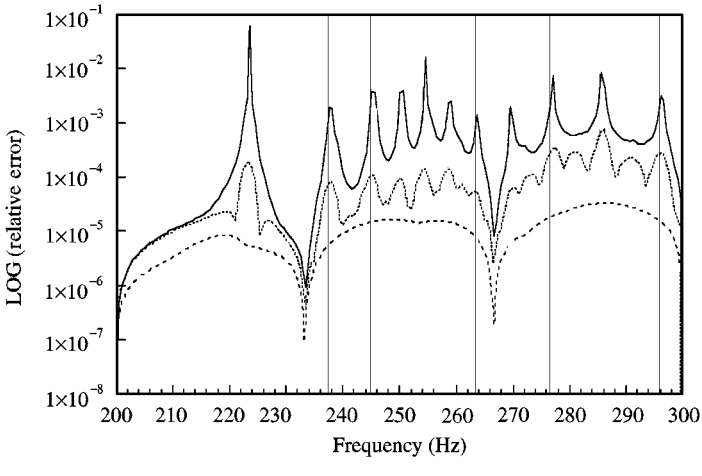

Figure 15. Real component of the relative error for the 4[pt] Lagrangian interpolation method comparing no damping (——) to 1% damping (- - - -) and 5% damping (– – – –).

both the real and imaginary responses for the "master" d.o.f. 51_x to those of the full d.o.f. solution found that the FWR reduced solutions were indistinguishable from the full d.o.f. response. This is seen in Figure 13, which shows both the real and imaginary response of the displacement magnitude of the "master" d.o.f. 51_x. The influence of the eigenvalues is clearly present for this case of 1% damping.

A comparison of the most stringent error criteria, the relative error, for the case in which there is no damping, to the cases with different percentages of critical damping demonstrates the effect that damping has on the overall response of this model, particularly the response near the eigenvalues. The relative error for the undamped case is compared to that of 1 and 5% damped cases (real components only) for the Hermitian (Figure 14) and the Lagrangian interpolation methods (Figure 15). These figures clearly show the gradual decrease and smoothing of the peaks at (near) the resonances. Also the comparison of the

% error of the displacement magnitude of the "master" d.o.f. 51_x for the undamped and damped cases shows that the overall error is approximately the same, at 0·01%. It appears that the accuracy of the FWR method is related to the % d.o.f. reduction, the interpolation window size and location, the sweep step size and the interpolation method used, and not whether the damping is present (at least for small % damping).

7. CONCLUSIONS

The preceding results show the successful implementation of the FWR methodology into a finite element environment. They demonstrate the validity and accuracy of the technique as applied to the structural acoustics analyses. They show, as well, the potential for the FWR methodology to improve such frequency analyses, including the use of the FWR method to extend and enhance the frequency analysis of the structural acoustic problems. This can be done simultaneously while reducing the computational costs associated with these types of analyses to a great extent.

The FWR method prototype algorithm, developed in standard Fortran 90, has been tested using FEM models generated by the ABAQUS FEM code. The most general formulation of the FWR method includes complex frequencies, complex frequency interpolation windows and damping. The use of parameter matrices, such as mass and stiffness, obtained from third party FEM codes such as ABAQUS, allows the existing FEM codes to generate the models directly for the FWR method.

The results given show that the FWR method may be used to optimize the d.o.f. reduction for a given model based on the accuracy and frequency of the window requirements. Re-ordering, according to a user-defined "master" node list, easily allows control of the d.o.f. of models. It permits preliminary analyses to be done to characterize the problem and response quickly, and to approximate the eigenvalues of the full d.o.f. system, without doing the eigenvalue analysis of the full d.o.f. model. The frequency windowing selection of interpolation points and interpolation methods can also be used to optimize the accuracy of the results versus the computational effort required. The frequency interpolation window location and the size can be selected to this end, as well as the variable placement of internal interpolation points with a selected window. This can be used to investigate first and then to narrow the regions of particular interest for the resultant system response. This choice of frequency windowing options, together with full frequency sweeps across an interpolation window, or partial frequency sweeps within an interpolation window, can further refine the analysis, as desired. Finally, multiple interpolation windows can be combined into a larger analysis window allowing the construction of the system response over a large frequency range from that of the individual smaller windows, with accuracy tailored as required for the smaller windows. The choice of interpolation methods can also be used to examine the system response at appropriate levels of accuracy, with little computational effort. The Lagrangian interpolation method is generally a less computational work, with a slightly reduced accuracy. The Hermitian interpolation method requires more computational effort, while it produces highly accurate results.

The FWR method, as implemented, minimizes computational effort by reuse of the calculated matrices. This important aspect of the method allows multiple analyses to be done without recalculation of the necessary matrices each time. For example, given the unordered mass, stiffness and damping matrices from an FEM code, different levels of d.o.f. reduction can be examined by changing the input "master" node list. Then, given this reordered set of matrices, a selected interpolation window is used to calculate the constructor matrices. These matrices are then valid for any frequency range within the

defined interpolation window. The constructor matrices do not need to be recalculated for any frequency sweep within this window, permitting a multiple frequency sweep analyses at different resolutions, with minimal computational cost. The same savings apply to the analyses for various loading and boundary conditions, which can be done without recalculation of the constructor matrices, permitting such analyses to be done at a minimal cost.

The varied aspects of the FWR method, as briefly discussed here, clearly have the potential to significantly impact the way frequency analyses are performed on large and complex models as applied to structural acoustic problems. This method, and its implementation as a computational tool, now offers a more effective and efficient environment, in which frequency sweeps of reduced models can be performed at greatly reduced computational cost while maintaining the requisite accuracy of the results. The direct incorporation of the resonance or modal response into the computational methodology will be undertaken and tested on FEM models. A final note. While this technique has been applied here to structural acoustic problems, the mathematics are such that the same techniques could be applied readily to other frequency-dependent problems, such as electromagnetic FEM models and inverse scattering problems, where the accuracy of calculations is also severely constrained by computational capabilities and costs.

ACKNOWLEDGMENTS

The authors would like to thank especially Dr. D. Lewis, III, of code 6354 at NRL, for his encouragement and support of this project. Author one and three gratefully acknowledge the support of the Office of Naval Research.

REFERENCES

1. R. D. COOK, D. S. MALKUS and M. E. PLESHA 1989 *Concepts and Applications of Finite Element Analysis*, 3rd edition New York: Wiley.
2. P. SESHU 1997 *Shock and Vibration* **4**, 199–210. Review: sub-structuring and component mode synthesis
3. L. D. FLIPPEN, JR 1994 *Computers and Mathematical Applications* **27**, 9–40. A theory of condensation model reduction.
4. L. D. FLIPPEN, JR 1994 *Computers and Mathematical Applications* **27**, 17–29. Current dynamics sub-structuring methods as approximations to condensation model reduction.
5. C. T. DYKA, R. P. INGEL and L. D. FLIPPEN, JR 1996 *Computers and Structures* **61**, 763–773. A new approach to dynamic condensation for FEM.
6. L. D. FLIPPEN, JR 1995 *Computers and Mathematical Applications* **29**, 39–52. Interpolation-based condensation of algebraic semi-discrete models with frequency response applications.
7. L. D. FLIPPEN, JR 2000 *U.S. Naval Research Laboratory Memo Report*. A generic bi-level formalism for unifying and extending model reduction methods, in press.
8. K. J. BATHE 1996. *Finite Element Procedures*. Englewood Cliffs, NJ: Prentice-Hall.
9. R. P. INGEL, C. T. DYKA and L. D. FLIPPEN, JR 1999 *U.S. Naval Research Laboratory Memo Report*, NAL/MR/6250-99-8402. Interpolation-based condensation model reduction part 1: frequency window reduction method.
10. T. M. R. ELLIS, I. R. PHILIPS and T. M. LAHEY 1994 *Fortran* 90 *Programming*. New York: Addison-Wesley.
11. *ABAQUS User's Examples, and Theory Manuals, Version* 5.6. 1996. *Hibbitt*, Pawtucket, RI: Karlsson and Sorensen.
12. *LAPACK Users' Guide* 1995, 2nd Edition, Society for Industrial and Applied Mathematics, Philadelphia, PA.